Journal of Applied Physics

Molecular tunneling in large tubes of 3D nitrogenated micropore materials

Cite as: J. Appl. Phys. **124**, 194303 (2018); https://doi.org/10.1063/1.5045194
Submitted: 18 June 2018 . Accepted: 01 November 2018 . Published Online: 20 November 2018

Artem Pimachev, and Yuri Dahnovsky

Molecular tunneling in large tubes of 3D nitrogenated micropore materials

Artem Pimachev and Yuri Dahnovsky[a)]
Department of Physics and Astronomy/3905, University of Wyoming, 1000 E. University Avenue, Laramie, Wyoming 82071, USA

(Received 18 June 2018; accepted 1 November 2018; published online 20 November 2018)

We study new 3D materials, π-conjugated microporous polymers (aza-CMPs), where 2D layers are connected by methanoic and ethanoic acid groups. The crystal parameters and the band structures are calculated. The energy gaps for a 3D crystal with the ethanoic ($E_g^{3D} = 1.04$ eV) and methanoic ($E_g^{3D} = 1.26$ eV) acid connecting groups are smaller than those for a 2D material ($E_g^{2D} = 1.64$ eV). The symmetry of a 3D crystal becomes lower than for a 2D aza-CMP by changing selection rules and optical spectra. The upper hole bands become non-degenerate for an aza-CMP with ethanoic acid and are doubly degenerate for an aza-CMP with methanoic acid connecting groups. The upper bands in the valence zone become more flat implying heavier hole masses that lead to lower hole mobilities. We also investigate molecular transport through the channels. We find that a CH_4 molecule moves easily along the tube in a large pore material and is hindered in a small pore (with ethanoic acid connecting groups) crystal. The ammonia molecule is attached to the tube walls with a large activation energy (about 0.39 eV). For the large molecules NR_4 (R=CH_3, C_2H_5), chemical reactions take place in the narrow tubes. In particular, an $N(CH_3)_4$ molecule decays in the fragments. The two atoms, N and C, are attached to the tube walls, and the three molecular fragments, CH_4, C_2H_6, and H_2, can further tunnel along the channels. The low energy gaps and tunable transport properties of π-conjugated microporous polymeric structures can be used for electronics, energy harvesting, gas separation, selective gas transport, hydrogen storage, and biomedicine (drug delivery). *Published by AIP Publishing.* https://doi.org/10.1063/1.5045194

I. INTRODUCTION

With new methodologies in synthesis, investigators have achieved much success in creating new 2D materials providing some control over electronic and mechanical properties expanding the range of applications to biomedicine,[1–9] nanoelectronics,[10–20] hydrogen, and energy storage.[21–30] One such material is π-conjugated microporous polymers (CMPs) where the pores are about 1 nm. g-C_2N 2D polyprophylene has recently attracted much interest. This material has a nitrogenated porous structure[31] with three benzene rings on a side of a hexagonal unit cell as shown in Fig. 1(a). If we continue the synthesis methodology, we arrive at a novel class of extended porous frameworks, which are known as π-conjugated microporous polymers shown in Fig. 1(b).

One of the most obvious applications of the large hole materials is to extend them to 3D crystals and consider large 3D tubes as channels for delivery molecules to designated places. This application is very important in medicine and hydrogen storage. Besides molecular transport, these materials have interesting electronic properties. Indeed, they are semiconductors. We study electronic properties as well. Because of low gap values, these materials can be used in energy harvesting (solar cells) and electronics.

II. MATERIALS DESCRIPTIONS

First, we describe some properties of 2D nitrogenated porous materials. The aza-CMP consists of five benzene rings on a side of the hexagon unit cell. An aza-CMP has been synthesized and its physical properties have been computationally studied within the *ab initio* approach. The first material, g-C_2N,[32–34] turns out to be a good semiconductor with a direct bandgap of 2.47 eV. This material has various applications, e.g., water-splitting photocatalysis.[35] The latter polymer, aza-CMP,[36,37] with a direct bandgap of 1.65 eV[38] is promising for the electric power supply and efficient energy storage.[39] In Ref. 40, it was shown that the gap can be tuned from 1.64 to 0.96 eV by replacing hydrogens by the halogen substituents varying from fluorine to iodine. The applications of the nitrogenated microporous materials are very broad. They can be useful as sensitizers in solar cells, for water splitting catalysis, in biomedicine, and for gas and energy storage. The next step forward in the study of aza-CMPs is to extend them to 3D materials where the aza-CMP 2D layers are connected by two different groups, methanoic and ethanoic acids, into a 3D crystal as shown in Fig. 2. The large 2D pores form the tubes in the third dimension that can be used, e.g., for a selective transport of various molecules and molecular groups.

In Figs. 3(a) and 3(b), we observe the picture for the ethanoic acid aza-CMP that is similar to the crystal structure of the methanoic acid aza-CMP shown in Figs. 4(a) and 4(b). In both the figures, we find hydrogen bonds that connect two adjacent layers. The methanoic acids and two adjacent layers are shown in Fig. 5. This figure clearly demonstrates that the two adjacent layers are connected by a hydrogen atom, which is bound to two oxygens forming the hydrogen bond. The methanoic and ethanoic acid connecting groups contain

[a)]Electronic address: yurid@uwyo.edu

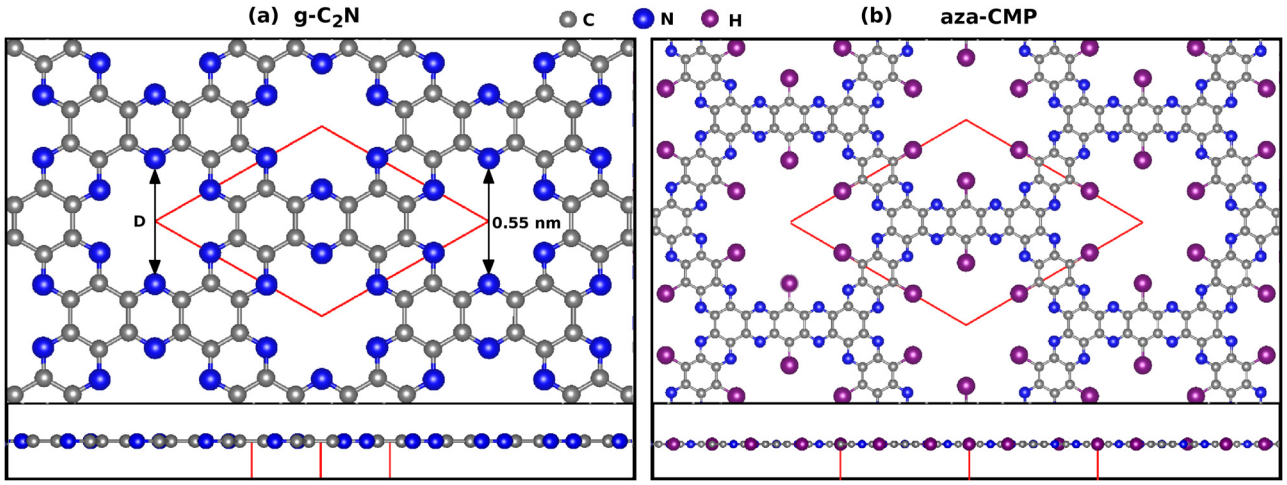

FIG. 1. Crystal structures of the nitrogenated porous materials: (a) g-C_2N with *three* nitrogenated benzene rings on a side of the unit cell and (b) X-aza-CMP (X = H) with *five* nitrogenated benzene rings on a side of the unit cell. The unit cells are presented in the red frames.

two oxygen atoms that, as we will see later, make them chemically active for some tunneling molecules. One of the most important applications of 3D aza-CMPs is to utilize their large-size micro-tubes for the transport of various molecules shown in Fig. 6. These molecules are methane CH_4 and NR_4 molecules with R = H, CH_3, and C_2H_5. Molecular transport will be studied in two different 3D materials with (a) methanoic acid connecting groups (see Fig. 4) and (b) ethanoic acid connecting groups (see Fig. 3). Before studying the transport properties of various molecules in two types of aza-CMPs, we first characterize them describing their electronic properties.

III. CALCULATION DETAILS

The electronic structure calculations and geometry optimizations have been performed in Vienna Ab Initio Simulation Package (VASP)[41,42] using the density functional theory (DFT) with the generalized gradient approximation (GGA). The projector augmented plane-wave (PAW) pseudopotential[43,44] with a cutoff energy of 400 eV has been employed for all calculations. The Γ-centered k-point grid has been generated from the Monkhorst-Pack scheme.[45] The structure relaxation for all 3D materials has been performed with the Pedrew-Burke-Ernzerhof (PBE) exchange-correlation functional[46] and 8 × 8 × 8 k-mesh grid using the conjugate gradient algorithm. Because of the long hydrogen bonds between two adjacent 2D layers (see Figs. 3–5), it is important to make the van der Waals (vdW) corrections to the exchange correlation functional. Thus, the van der Waals corrections have been incorporated using the DFT-D2 method due to its better description of long-range vdW interactions.[47–49] The band structure has been calculated with the Heyd-Scuseria-Ernzerhof (HSE06) hybrid exchange-correlation functional. For the band structure calculations, we have used the M-Γ-K-M path in a k-space. For the calculations along this path, we have chosen 60 k-points in total. The transport energy barriers were computed by restricting one dimension of the center ion and discretely changing it along the tube keeping all the other dimension constraints free.

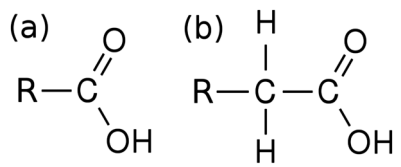

FIG. 2. (a) Methanoic and (b) ethanoic acids.

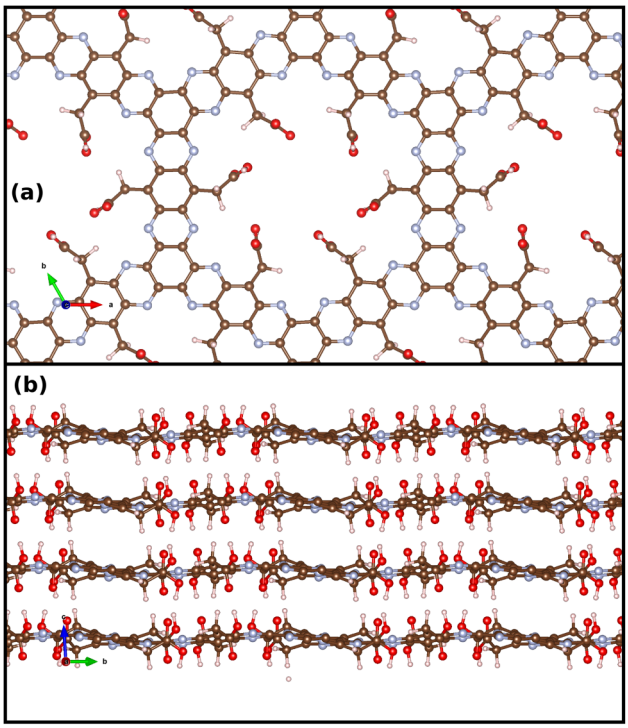

FIG. 3. aza-CMP with *five* nitrogenated benzene rings on a side of the unit cell. The connecting group is *ethanoic acid*. (a) The plane cross-section and (b) the cross-section along a *z*-axis.

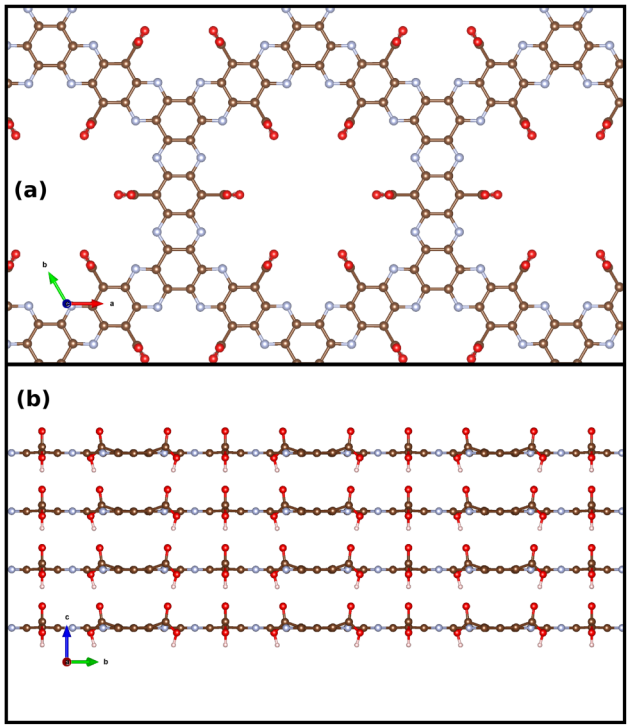

FIG. 4. Crystal structures of the aza-CMP with *five* nitrogenated benzene rings on a side of the unit cell. The connecting group is *methanoic acid*. (a) The in-plane cross-section and (b) the cross-section along a z-axis.

IV. ELECTRONIC PROPERTIES AND MOLECULAR TRANSPORT

A. Electronic structure

The two 3D aza-CMPs depicted in Figs. 3 and 4 are novel materials, whose geometries and electronic properties are unknown. Thus, we first study their crystal structures

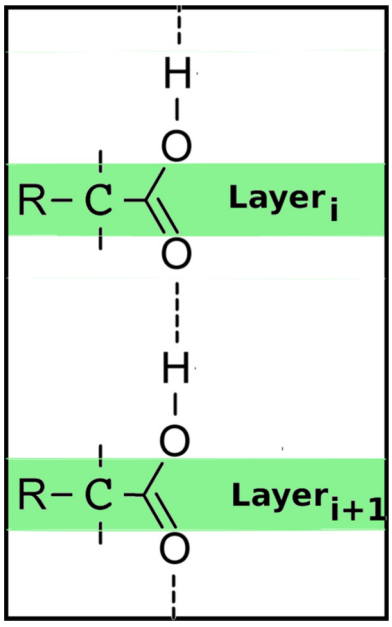

FIG. 5. Two layers are connected by the methanoic acid group with the hydrogen bond formation.

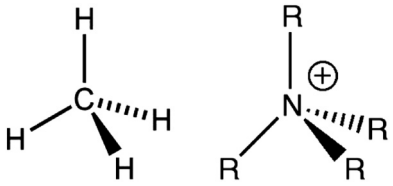

FIG. 6. Left figure depicts a methane molecule, CH_4. The right figure shows a general molecule with the different substitution groups. In particular, R=H, CH_3, and C_2H_5.

providing the crystal parameters. After the optimization, we have found that the crystal structure for a crystal with the methanoic acid connecting group is trigonal with the following crystal unit lattice constants: $a = 16.55$ Å, $b = 16.55$ Å, and $c = 4.57$ Å and angles $\alpha = 90.04°$, $\beta = 90.03°$, and $\gamma = 120.00°$. For the ethanoic acid connecting group, a crystal structure is triclinic where the crystal parameters are $a = 16.55$ Å, $b = 16.48$ Å, and $c = 4.65$ Å with $\alpha = 94.43°$, $\beta = 86.75°$, and $\gamma = 120.07°$.

When the crystal parameters of the 3D aza-CMPs under study are known, we investigate the electronic properties of these materials. In particular, we provide their band structures and compare them with the known band structure of a 2D aza-CMP. The band structures for both materials have the direct gaps at the Γ-point as shown in Figs. 7(b) and 7(c). The bands look similar to those of a 2D aza-CMP shown in Fig. 7(a).

From Figs. 7(a)–7(c), at a closer look, we see that the band structures are different. *First*, the bandgap values are $E_g^{2D} = 1.64$ eV for a 2D layer [see Fig. 7(a)],[38,40] $E_g^{3D} = 1.04$ eV [see Fig. 7(b)], and $E_g^{3D} = 1.26$ eV [see Fig. 7(c)] for 3D crystals with the *ethanoic* acid and *methanoic* acid connecting groups, respectively. The largest energy gap difference is $\Delta E = E_g^{2D} - E^{3D} = 0.60$ eV. *Second*, we know[40] that a 2D crystal has a D_{6h} symmetry at the Γ-point, whereas the same symmetry in a 3D crystal is lower. Indeed, it is only C_{3v} for a 3D aza-CMP with the methanoic and C_3 for an aza-CMP with the ethanoic acid connecting groups, respectively. For the 2D and 3D aza-CMPs with methanoic connecting groups, we observe doubly degenerate upper hole bands because both symmetry groups D_{6h} and C_{3v} have two-dimensional group representations. However, for the 3D aza-CMP with the ethanoic acid connecting group, the doubly degenerate upper hole bands are transformed into two non-degenerate bands because the representations of a C_3 group are only one dimensional. There is a *third* feature, which we observe from the valence band structure—the hole bands become more flat for a 3D case implying the heavier hole effective masses. As far as effective electron masses are concerned, they remain almost unchanged.

B. Molecular transport

One of the most important applications of 3D aza-CPMs is molecular transport in long channels. Indeed, the nanopores are large enough to allow some large molecules to tunnel through the wide tubes. Such tunneling could have an

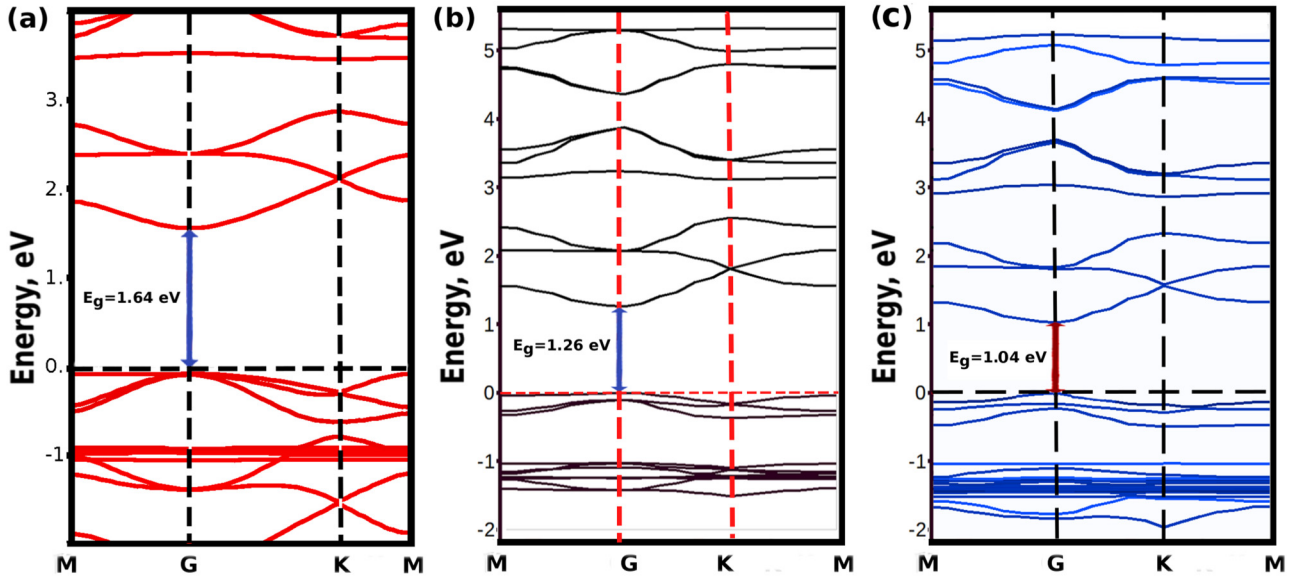

FIG. 7. Band structures of (a) 2D aza-CMP, (b) 3D aza-CMP with a methanoic acid connecting group, and (c) 3D aza-CMP with an ethanoic acid connecting group.

application in biomedicine for drug delivery, where a large molecule can be delivered to specific places by tunneling through a 3D aza-CMP channel.

In this work, we study various molecules that are different in sizes, electron affinities, and chemically active groups. In particular, we consider the following molecules: (a) CH_4, (b) NH_4, (c) $N(CH_3)_4$, and $N(C_2H_5)_4$, schematically shown in Fig. 6. In Fig. 8, we demonstrate how a molecule moves in the large and small diameter nano-pores. The left figure represents the reactant state for the tunneling of a $N(C_2H_5)_4$ molecule in a wide tube. The right figure demonstrates the reactant state of a smaller molecule, CH_4 tunneling in a narrow tube.

The process of a molecule transport is schematically shown in Fig. 9. The molecule moves along the tube. The first part of the low picture represents the lowest energy state of the particle, the particle is between the layers. In the lower middle picture, the particle is passing the layer. This picture provides the maximum value in the activation energy. Then, the particle is in between the layers again. This particle transport picture is periodic with the lattice constant along the z-axis. The activation energy is defined as the energy at the saddle point between the 2D layers. We have calculated the activation energies for various scenarios. The criterion for a molecule to move along a tube is that the activation energy is about or less than the room temperature, i.e.,

$$E_a \leq k_B T = 25\,\text{meV}. \tag{1}$$

The activation energies are given in Table I. As expected, the CH_4 molecule easily tunnels through the large aza-CMP pores with the barrier energy lesser than the room temperature. However, in the small-size aza-CMP pores, the transport becomes much less efficient. From column 1 in Table I, all molecules have the lower barriers and, therefore, do not dissociate. The barriers for the larger molecules are very high and, thus, these molecules practically do not tunnel. The physical

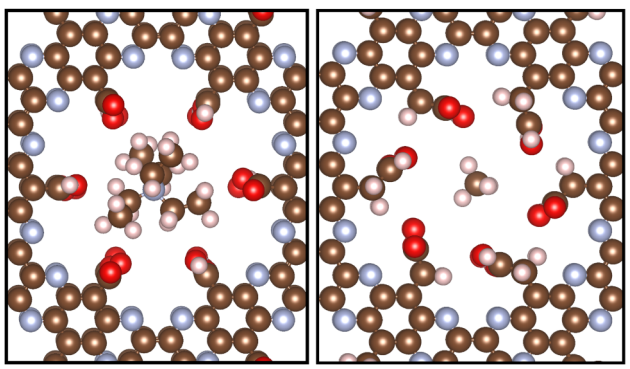

FIG. 8. Molecules in the reactant states of the tunneling through the nanotubes. (a) $N(C_2H_5)_4$ (the left-hand side) and (b) CH_4 (the right-hand side).

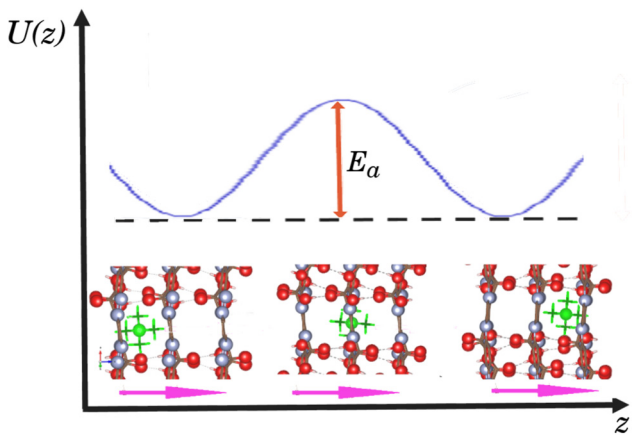

FIG. 9. A schematic picture of the molecular tunneling along the tube.

TABLE I. Transport activation and bond dissociation energies for various tunneling molecules in the large and small pore 3D aza-CMPs.

	Activation energy (meV) (large pores)	Activation energy (meV) (small pores)	Dissociation energy (eV) $\mathcal{E}_r - \mathcal{E}_p$
CH_4	20.6	77.2	No dissociation
NH_4	87.7	389	4.49
$N(CH_3)_4$	209	Chemical reaction	9.07
$N(C_2H_5)_4$	788	Chemical reaction	Chemical reaction

picture becomes rather different for molecular tunneling through the narrow tubes. Only CH_4 molecules do not dissociate, while all other molecules either get attached to a tube wall or chemically react with the 3D-aza-CMPs. For the large molecules, the transport activation energies are very high; therefore, the molecules do not tunnel. The NH_4 molecule sticks to the tube wall with the bond dissociation energy of 0.39 eV as shown in Fig. 10(b). To make sure that our calculations are correct, we have also compared the computed dissociation energy with the ones found in Ref. 50. A very good agreement has been found.

By studying the tunneling of various molecules, we have found that some molecules despite their small size can be stuck to the walls of the tube. In particular, the NH_4 molecule is attached to the narrow tube wall as shown in Fig. 10.

Furthermore, there is another special case that we would like to emphasize. For the transport of a $N(CH_3)_4$ molecule, a chemical reaction takes place in a large tube. The large molecule decays into several fragments: CH_4, C_2H_6, NH, and C_2H_2 as shown in Fig. 11. Apparently, the atoms N and C react with the tube walls, while

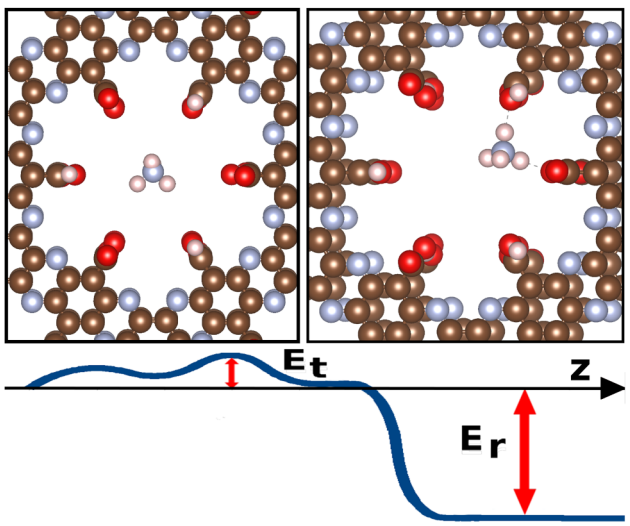

FIG. 10. Reactant and product states are presented in the left and right upper figures. The lower figure shows the energy dependence on the reaction coordinate.

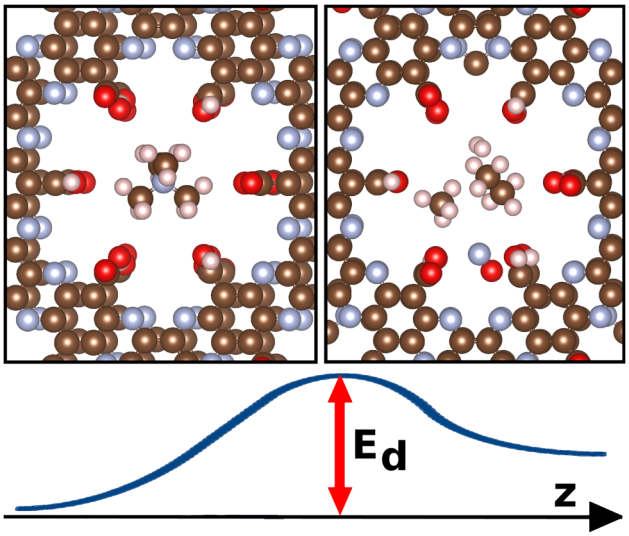

FIG. 11. Reactant and product states are presented in the left and right upper figures. The lower figure shows the energy behavior along the reaction coordinate.

the CH_4, C_2H_6, and H_2 molecules can move through the pores.

V. CONCLUSIONS

In this work, we have studied novel 3D aza-CMP crystals, which are formed from the aza-CMP layers shown in Fig. 1(b). To connect the 2D layers into a 3D crystal, we have used the methanoic and ethanoic acid connecting groups as shown in Figs. 2(a) and 2(b), respectively. Two adjacent layers are connected by a hydrogen bond, and the hydrogen atom between the two oxygens is shown in Fig. 5. We have characterized these materials by calculating their lattice parameters and energy band structures as depicted in Fig. 7. *First*, we have found that the energy gaps for the crystal with the ethanoic and methanoic acid connecting groups are significantly lower than that for a 2D crystal. The gap values are $E_g^{2D} = 1.64$ eV for 2D aza-CMP and $E_g^{3D} = 1.26$ eV and $E_g^{3D} = 1.04$ eV for 3D aza-CMPs with methanoic and ethanoic acid connecting groups, respectively. Besides the energy gap shrinking, there is a *second* important effect. The symmetry of the crystal becomes lower for a 3D material than that for a 2D aza-CMP, thereby changing selection rules and optical spectra. The *third* effect is that the upper hole bands become non-degenerate for the 3D aza-CMP with ethanoic acid connecting group while being doubly degenerate for the 2D aza-CMP and 3D aza-CMP with methanoic acid connecting group as shown in Fig. 7. The *fourth* effect is that the upper bands in the valence zone become more flat implying heavier hole masses that lead to lower hole mobilities.

Furthermore, we have investigated the transport of various molecules (see Fig. 6) through the channels in 3D crystals. We have found that CH_4 molecule moves easily along the wide tubes and is hindered in the narrow tube materials. The transport activation and dissociation energies are given in Table I. Besides the molecular tunneling, there

are some other interesting phenomena taking place in molecular transport through the tubes. We have found that the ammonia molecule can get attached to the tube walls. Indeed, as follows from Table I, the activation energy for the ammonia molecule to further move along the narrow tube is very large (about 0.39 eV). Thus, the molecule attaches to a tube wall with a dissociation energy of 4.5 eV. For the larger molecules, the situation is more complicated where the chemical reactions take place during the tunneling process. As shown in Fig. 11, $N(CH_3)_4$ molecule decays into N and C, which further react with the tube walls and three molecular fragments, CH_4, C_2H_6, and H_2, which can tunnel further along the channels. The latter effect is very important in biomedical applications, such as drug delivery. By varying the pore sizes and the tunneling molecules, we are able to selectively transport particular molecules to a designated place that includes gas separation and hydrogen storage. The low energy gaps and tunable transport properties of π-conjugated microporous polymeric structures can also be used for energy harvesting (solar cells) and electronics.

ACKNOWLEDGMENTS

This work has been supported by a grant (No. DMR-1710512) from the U.S. National Science Foundation to the University of Wyoming.

[1]Y. Chen, Z. P. Michael, G. P. Kotchey, Y. Zhao, and A. Star, ACS Appl. Mater. Interfaces **6**, 3805 (2014).
[2]S. K. Singh, M. K. Singh, P. P. Kulkarni, V. K. Sonkar, J. J. Grácio, and D. Dash, ACS Nano **6**, 2731 (2012).
[3]R. Rauti, N. Lozano, V. Leon, D. Scaini, M. Musto, I. Rago, F. P. Ulloa Severino, A. Fabbro, L. Casalis, E. Vazquez *et al.*, ACS Nano **10**, 4459 (2016).
[4]C. Chung, Y.-K. Kim, D. Shin, S.-R. Ryoo, B. H. Hong, and D.-H. Min, Acc. Chem. Res. **46**, 2211 (2013).
[5]Y. Toumia, S. Orlanducci, F. Basoli, S. Licoccia, and G. Paradossi, J. Phys. Chem. B **119**, 2051 (2015).
[6]A. B. Seabra, A. J. Paula, R. de Lima, O. L. Alves, and N. Duran, Chem. Res. Toxicol. **27**, 159 (2014).
[7]N. Mohanty and V. Berry, Nano Lett. **8**, 4469 (2008).
[8]Q. Mu, G. Su, L. Li, B. O. Gilbertson, L. H. Yu, Q. Zhang, Y.-P. Sun, and B. Yan, ACS Appl. Mater. Interfaces **4**, 2259 (2012).
[9]V. T. Pham, V. K. Truong, M. D. Quinn, S. M. Notley, Y. Guo, V. A. Baulin, M. Al Kobaisi, R. J. Crawford, and E. P. Ivanova, ACS Nano **9**, 8458 (2015).
[10]P. Miró, M. Audiffred, and T. Heine, Chem. Soc. Rev. **43**, 6537 (2014).
[11]G. Fiori, F. Bonaccorso, G. Iannaccone, T. Palacios, D. Neumaier, A. Seabaugh, S. K. Banerjee, and L. Colombo, Nat. Nanotechnol. **9**, 768 (2014).
[12]K. Novoselov, D. Jiang, F. Schedin, T. Booth, V. Khotkevich, S. Morozov, and A. Geim, Proc. Natl. Acad. Sci. U.S.A. **102**, 10451 (2005).
[13]Y.-W. Son, M. L. Cohen, and S. G. Louie, Nature **444**, 347 (2006).
[14]G. Peng, J. E. Ellis, G. Xu, X. Xu, and A. Star, ACS Appl. Mater. Interfaces **8**, 7403 (2016).
[15]C.-H. Liu, Q. Chen, C.-H. Liu, and Z. Zhong, Nano Lett. **16**, 1064 (2016).
[16]A. Du, Z. Zhu, and S. C. Smith, J. Am. Chem. Soc. **132**, 2876 (2010).
[17]R. S. Sundaram, M. Steiner, H.-Y. Chiu, M. Engel, A. A. Bol, R. Krupke, M. Burghard, K. Kern, and P. Avouris, Nano Lett. **11**, 3833 (2011).
[18]J. Woo, K.-H. Yun, and Y.-C. Chung, ACS Appl. Mater. Interfaces **8**, 10477 (2016).
[19]Z. Qin, M. Taylor, M. Hwang, K. Bertoldi, and M. J. Buehler, Nano Lett. **14**, 6520 (2014).
[20]C. Berger, Z. Song, T. Li, X. Li, A. Y. Ogbazghi, R. Feng, Z. Dai, A. N. Marchenkov, E. H. Conrad, P. N. First *et al.*, J. Phys. Chem. B **108**, 19912 (2004).
[21]C. Zhou and J. A. Szpunar, ACS Appl. Mater. Interfaces **8**, 25933 (2016).
[22]C. Zhou, J. A. Szpunar, and X. Cui, ACS Appl. Mater. Interfaces **8**, 15232 (2016).
[23]T. Takamura, K. Endo, L. Fu, Y. Wu, K. J. Lee, and T. Matsumoto, Electrochim. Acta **53**, 1055 (2007).
[24]S.-H. Park, H. J. Kim, J. Lee, Y. K. Jeong, J. W. Choi, and H. Lee, ACS Appl. Mater. Interfaces **8**, 13973 (2016).
[25]Z. Xing, Y. Qi, Z. Jian, and X. Ji, ACS Appl. Mater. Interfaces **9**, 4343 (2016).
[26]Y. Jiang, Z.-J. Jiang, L. Yang, S. Cheng, and M. Liu, J. Mater. Chem. A **3**, 11847 (2015).
[27]J. Shui, Y. Lin, J. W. Connell, J. Xu, X. Fan, and L. Dai, ACS Energy Lett. **1**, 260 (2016).
[28]X. Zhao, C. M. Hayner, M. C. Kung, and H. H. Kung, ACS Nano **5**, 8739 (2011).
[29]E. D. Walsh, X. Han, S. D. Lacey, J.-W. Kim, J. W. Connell, L. Hu, and Y. Lin, ACS Appl. Mater. Interfaces **8**, 29478 (2016).
[30]Q. Zhou, M. Zhang, J. Chen, J.-D. Hong, and G. Shi, ACS Appl. Mater. Interfaces **8**, 20741 (2016).
[31]M. Bieri, M. Treier, J. Cai, K. Aït-Mansour, P. Ruffieux, O. Gröning, P. Gröning, M. Kastler, R. Rieger, X. Feng *et al.*, Chem. Commun. **45**, 6919 (2009).
[32]J. Mahmood, E. K. Lee, M. Jung, D. Shin, I.-Y. Jeon, S.-M. Jung, H.-J. Choi, J.-M. Seo, S.-Y. Bae, S.-D. Sohn *et al.*, Nat. Commun. **6**, 6486 (2015).
[33]M. Yagmurcukardes, S. Horzum, E. Torun, F. M. Peeters, and R. T. Senger, Phys. Chem. Chem. Phys. **18**, 3144 (2016).
[34]S. Guan, Y. Cheng, C. Liu, J. Han, Y. Lu, S. A. Yang, and Y. Yao, Appl. Phys. Lett. **107**, 231904 (2015).
[35]H. Wang, X. Li, and J. Yang, ChemPhysChem **17**, 2100 (2016).
[36]Z.-D. Yang, W. Wu, and X. C. Zeng, J. Mater. Chem. C **2**, 2902 (2014).
[37]V. Briega-Martos, A. Ferre-Vilaplana, A. de la Pena, J. L. Segura, F. Zamora, J. M. Feliu, and E. Herrero, ACS Catal. **7**, 1015 (2016).
[38]L. Wang, Y. Wan, Y. Ding, Y. Niu, Y. Xiong, X. Wu, and H. Xu, Nanoscale **9**, 4090 (2017).
[39]Y. Kou, Y. Xu, Z. Guo, and D. Jiang, Angew. Chem. **123**, 8912 (2011).
[40]A. Pimachev, V. Proshchenko, and Y. Dahnovsky, J. Appl. Phys. **122**, 115305 (2017).
[41]G. Kresse and J. Furthmüller, Comput. Mater. Sci. **6**, 15 (1996).
[42]G. Kresse and J. Furthmüller, Phys. Rev. B **54**, 11169 (1996).
[43]G. Kresse and D. Joubert, Phys. Rev. B **59**, 1758 (1999).
[44]P. E. Blöchl, Phys. Rev. B **50**, 17953 (1994).
[45]H. J. Monkhorst and J. D. Pack, Phys. Rev. B **13**, 5188 (1976).
[46]J. P. Perdew, K. Burke, and M. Ernzerhof, Phys. Rev. Lett. **77**, 3865 (1996).
[47]W. Hu, X. Wu, Z. Li, and J. Yang, Phys. Chem. Chem. Phys. **15**, 5753 (2013).
[48]X. Chen, F. Tian, C. Persson, W. Duan, and N.-x. Chen, Sci. Rep. **3**, 3046 (2013).
[49]S. Grimme, J. Comput. Chem. **27**, 1787 (2006).
[50]Y.-R. Luo, *Comprehensive Handbook of Chemical Bond Energies* (CRC Press, 2007).